• Original Paper •

Comparison of PM$_{2.5}$ and CO$_2$ Concentrations in Large Cities of China during the COVID-19 Lockdown

Chuwei LIU[1], Zhongwei HUANG[1], Jianping HUANG[*1,2], Chunsheng LIANG[1], Lei DING[1],
Xinbo LIAN[1], Xiaoyue LIU[1], Li Zhang[1], and Danfeng WANG[1]

[1]*Collaborative Innovation Center for Western Ecological Safety (CIWES), College of Atmospheric Sciences,*
Lanzhou University, Lanzhou 730000, China
[2]*CAS Center for Excellence in Tibetan Plateau Earth Sciences, Beijing 100101, China*

ABSTRACT

Estimating the impacts on PM$_{2.5}$ pollution and CO$_2$ emissions by human activities in different urban regions is important for developing efficient policies. In early 2020, China implemented a lockdown policy to contain the spread of COVID-19, resulting in a significant reduction of human activities. This event presents a convenient opportunity to study the impact of human activities in the transportation and industrial sectors on air pollution. Here, we investigate the variations in air quality attributed to the COVID-19 lockdown policy in the megacities of China by combining in-situ environmental and meteorological datasets, the Suomi-NPP/VIIRS and the CO$_2$ emissions from the Carbon Monitor project. Our study shows that PM$_{2.5}$ concentrations in the spring of 2020 decreased by 41.87% in the Yangtze River Delta (YRD) and 43.30% in the Pearl River Delta (PRD), respectively, owing to the significant shutdown of traffic and manufacturing industries. However, PM$_{2.5}$ concentrations in the Beijing-Tianjin-Hebei (BTH) region only decreased by 2.01% because the energy and steel industries were not fully paused. In addition, unfavorable weather conditions contributed to further increases in the PM$_{2.5}$ concentration. Furthermore, CO$_2$ concentrations were not significantly affected in China during the short-term emission reduction, despite a 19.52% reduction in CO$_2$ emissions compared to the same period in 2019. Our results suggest that concerted efforts from different emission sectors and effective long-term emission reduction strategies are necessary to control air pollution and CO$_2$ emissions.

Key words: PM$_{2.5}$, CO$_2$ emissions, lockdown measures, traffic emission, industrial activity

Citation: Liu, C. W., and Coauthors, 2022: Comparison of PM$_{2.5}$ and CO$_2$ concentrations in large cities of China during the COVID-19 lockdown. *Adv. Atmos. Sci.*, https://doi.org/10.1007/s00376-021-1281-x.

Article Highlights:

- During the COVID-19 lockdown in China, The concentrations of PM$_{2.5}$ in southern (northern) China decreased significantly (slightly).
- Both weather conditions and reduced industrial intensity were important reasons for the different changes in PM$_{2.5}$ concentrations in various urban agglomerations.
- The CO$_2$ emissions decreased in China but had little effect on reducing CO$_2$ concentration.
- Short-term lockdowns cannot reduce CO$_2$ concentrations in the atmosphere effectively.

---

1. Introduction

Environmental pollution is among the most serious problems threatening China's densely populated cities. Particulate matter smaller than 2.5 μm (PM$_{2.5}$) is of particular concern due to its serious impact on human health (Tang et al., 2020) and its role in climate change (Guo et al., 2017). The formation of PM$_{2.5}$ in large cities in China is mainly caused by anthropogenic emissions related to industrial production, agriculture, transportation, and activities related to daily life.

Changes in urban air quality are attainable by various policy implementations, including restrictions on vehicle movement. During the 2008 Beijing Olympics, restrictions on private vehicles were implemented in Beijing, which reduced the mobile source emissions of NO$_x$ and NMVOCs by 46% and 57%, respectively (Wang et al., 2010). During the Asia-Pacific Economic Cooperation (APEC) Summit in 2014, Beijing restricted daily vehicle use, postponed the provi-

---

* Corresponding author: Jianping HUANG
  Email: hjp@lzu.edu.cn

sion of central heating, and closed construction sites (Liu et al., 2017); consequently, the emissions of various pollutants dropped significantly. Starting in January 2020, Chinese cities adopted a range of policies, including community lockdown and delays in resuming work and reopening schools, to curb the further spread of COVID-19. The traffic volume in densely populated cities declined significantly due to these measures. However, the specific control measures adopted during the spread of COVID-19, the 2008 Beijing Olympic Games, and the APEC meeting differ. In addition to controlling the traffic volume, the industry, construction, and coal burning were also imposed during the Beijing Olympic Games, and the APEC meeting. The city lockdown during COVID-19 generally reduced the traffic volume, while other industries may not have been suspended to a large extent. Therefore, the city lockdown caused by COVID-19 provides a valuable opportunity to assess the contribution of traffic emissions and other factors affecting $PM_{2.5}$ concentrations in large cities.

Overall, the $PM_{2.5}$ concentration in China has dropped significantly over the last decade (Chu et al., 2021). The $PM_{2.5}$ concentration in Wuhan, which had the most stringent lockdown measures, experienced the most significant declines (Yao et al., 2021). The substantial reduction in emissions in various sectors (industry, transportation, human activities, etc.) is the main reason for the decline in $PM_{2.5}$. In addition, the reduction in traffic caused a significant drop in NO_2 concentrations. The concentrations of $PM_{2.5}$ and NO_2 showed relatively consistent changes. The reduction in the NO_x hinders the formation of secondary aerosols, which is conducive to reduced $PM_{2.5}$ concentration (Chu et al., 2021). However, the nature of the $PM_{2.5}$ concentration changes in different regions varies (Pei et al., 2020). Southern cities had a stronger controlling effect on $PM_{2.5}$ than northern cities (Lu et al., 2021). For large southern cities such as Shanghai, $PM_{2.5}$ concentration dropped significantly (Chen et al., 2020), while the $PM_{2.5}$ concentration in the BTH region remained high (Sulaymon et al., 2021). The abnormal changes in the $PM_{2.5}$ concentration in BTH are partially attributed to unfavorable weather conditions, noting that the pollutants cannot be quickly diffused or removed under conditions of high temperature, high humidity, and low wind speeds, the combination of which keeps the concentration of urban pollutants at high levels (Wang et al., 2020; Sulaymon et al., 2021). Meanwhile, heating, coal burning, and local industrial activities also impact emissions (Nichol et al., 2020; Dai et al., 2021). Therefore, the root cause of the different $PM_{2.5}$ concentration changes in different regions is complex. Therefore, it is necessary to further explore the anthropogenic component of $PM_{2.5}$ pollution in different regions of China during the city lockdowns.

During the city lockdowns, CO_2 emissions were also affected. Many studies have shown that the industrial sector (An et al., 2018), transportation sectors (Yuan et al., 2019), and other sectors that use fossil fuels contribute substantially to CO_2 emissions. In recent years, densely popu-

lated and economically developed eastern cities in China have experienced more significant growth in CO_2 emissions than in the less populated western cities (Chen and Yang, 2015). With the changes in the intensity of industrial and transportation activities in large cities and their surrounding areas during the city lockdown, CO_2 emissions by various departments and regions may also change to varying degrees. Studies on the global (Bertram et al., 2021) and European (Andreoni, 2021) regions also showed that CO_2 emissions dropped significantly during the lockdown. Nevertheless, the effect of emission reduction in reducing the overall CO_2 concentration and its effect on the climate is not obvious since it is an overall complicated process (Sovacool et al., 2020).

This study compares the characteristics and the causes in the changes of $PM_{2.5}$ concentration in three large Chinese city clusters, Beijing-Tianjin-Hebei (BTH), the Yangtze River Delta (YRD), and the Pearl River Delta (PRD) over 2015–20, especially during the city lockdown in 2020. In addition, the change in CO_2 emissions and its impact on the CO_2 concentration in the environment are analyzed. This article aims to provide feasible measures for cities to reduce air pollution and CO_2 emissions.

2.   Data and methods

2.1. NO_2 and $PM_{2.5}$ concentration data

The NO_2 and $PM_{2.5}$ concentration data came from the Qingyue Open Environmental Data Centre (data.epmap.org). The data on this website are derived from the real-time air quality publishing system of the Environmental Monitoring Station of the Ministry of Environmental Protection. The periods considered in this research were from 24 January to 23 February 2020—the first month after the lockdown of urban residential areas in that year—and every 24 January to 23 February in 2015–19. The NO_2 and $PM_{2.5}$ concentration data were measured hourly, and the subsequent dataset constitutes the average of the hourly data of the state-controlled sites in the specific cities (HG663-2013). The NO_2, and $PM_{2.5}$ data used in this study were the averages of the hourly data for each city during the period. We used Student-T test to measure the significance of the difference in pollutant concentration changes between 2015–19 and 2020.

2.2.   Fire radiative power data

The fire radiative power (FRP) data which reflects the industrial activities in this study, were extracted from the Suomi-NPP/VIIRS VNP14IMGTDL standard dataset (https://earthdata.nasa.gov/earth-observation-data/near-real-time/firms/v1-vnp14imgt#ed-viirs-375m-attributes). The data were collected by the Visible Infrared Imaging Radiometer Suite (VIIRS) on the Suomi National Polar-orbiting Partnership (S-NPP) satellite. The S-NPP is managed by the National Aeronautics and Space Administration (NASA) and the National Oceanic and Atmospheric Adminis-

tration (NOAA). The satellite can monitor ground-based thermal anomalies twice a day, once in the daytime, once at night, with a monitoring resolution of up to 375 m. The FRP of the thermal anomaly point is calculated using the M13 channel. The satellite can identify temperatures between 400 K and 1200 K (Schroeder et al., 2014). The thermal radiation peak of industrial combustion is in the mid-infrared band. The thermal anomaly is extracted according to the difference between its thermal radiation energy and the ambient temperature (Sun et al., 2018; Tsidulko et al., 2018). The emission error in eastern China is 1.2% (Schroeder et al., 2014). The observed fire points are divided into four types: presumed vegetation fire, an active volcano, other static land sources, and offshore detection (which include all detections over water). We selected only those fire points in the "other static land source" category. Among these fire points, those that fall in urban and rural areas, residential areas, and those attributed to industry and mining were selected based on China's 2018 land-use remote sensing monitoring data (https://www.resdc.cn/Default.aspx).

To eliminate the influence of factors such as radiation and daytime living sources, we selected the nocturnal data from 0100 to 0400 LST (local standard time, LST=UTC+8). Past industrial heat source extraction studies also selected nighttime thermal anomaly data (Ma et al., 2018; Wang et al., 2018; Sun et al., 2020). The FRP values of the fire points in the 0.1° × 0.1° area at that moment were accumulated, and the FRP value of the day was obtained, reflecting the degree of industrial activities on that day. The daily FRP value for each area in the study period was then summed to reflect the degree of industrial activities for that period. The cumulative FRP value of each region in 2020 was subtracted from that of 2019, reflecting the difference in industrial activities in 2020 compared with 2019.

2.3. *Location, population, transportation and economy of the researched area*

The BTH, YRD, and the PRD regions are located in North, Southeast, and South China, respectively (Fig. 1). Using the urban population data of the *China City Construction Statistical Yearbook 2017*, cities with populations greater than 1.5 million in the urban areas of BTH, TRD, and PRD were classified as "large cities". The BTH region
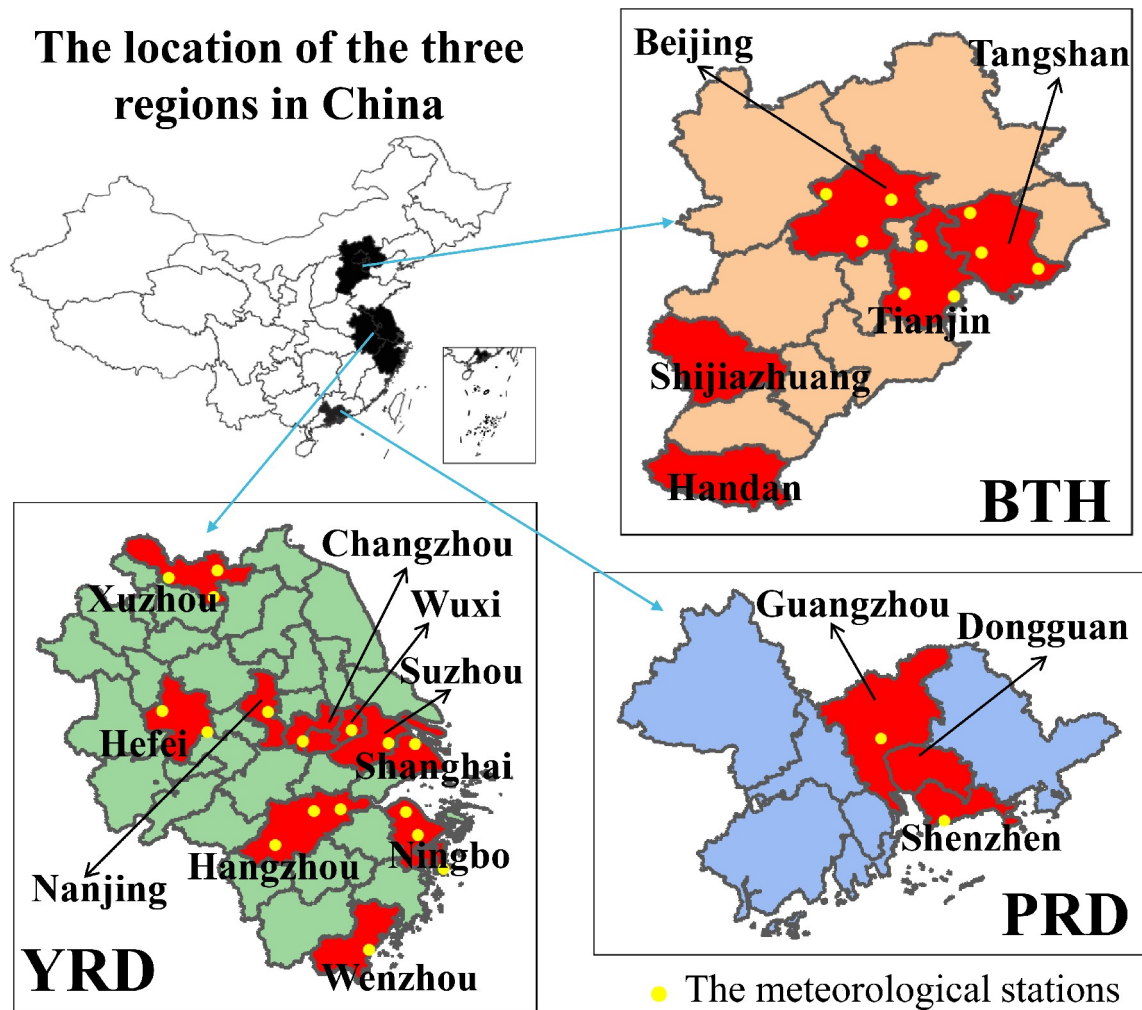
Fig. 1. Location map of the BTH, YRD, and PRD. The red areas are "big cities", and the meteorological stations in these cities are marked with yellow dots.

comprises five cities (Beijing, Tianjin, Shijiazhuang, Handan, and Tangshan), the YRD comprises ten cities (Suzhou, Wuxi, Hefei, Changzhou, Wenzhou, Xuzhou, Hangzhou, Nanjing, Shanghai, and Ningbo), and the PRD comprises three cities (Dongguan, Guangzhou, and Shenzhen). Figure 1 shows the location of these cities. The sales value of the manufacturing and mining industries for the three regions was based on the 2016 data sourced from the *China Industry Yearbook 2017*. The annual primary energy production and the annual power generation composition were based on 2017 data sourced from the *China Energy Statistical Yearbook-2018*. The above values for the unit area were then calculated. The calculation of the administrative area was based on 2017 data sourced from the *China City Statistical Yearbook 2018*. We adopted the average data of Guangdong Province as the data of the PRD. The transportation volume data of road passengers and cargo were derived from the Ministry of Transport of the People's Republic of China (http://www.mot.gov.cn/). The GDP data came from China's National Bureau of Statistics (https://data.stats.gov.cn/).

2.4. *Meteorological conditions*

The daily-averaged temperature, relative humidity, and wind speed data were obtained from the China Surface Climate Data Daily Value Data Set (V3.0) compiled by the China Meteorological Data Service Center (http://data.cma.cn/data/cdcindex/cid/6d1b5efbdcbf9a58.html). These data were measured from 28 of China's 699 benchmark and basic meteorological stations (Fig. 1). They are all located in the 18 major cities listed in section 2.3 (but not all cities have meteorological stations).

2.5. *CO$_2$ emission data*

Data of CO$_2$ emitted by various sectors during the city lockdown were from the Carbon Monitor project (https://car-bonmonitor.org.cn/). The CO$_2$ emissions data for 2008–18 were from the provincial CO$_2$ emission inventory provided by the Carbon Emission Accounts & Datasets (CEADs, https://www.ceads.net.cn/data/province/) (Liu, et al., 2020a, b; Shan et al., 2016, 2018, 2020). The CO$_2$ concentration data were based on the GOSAT dataset in GOSAT/GOSAT-2 EORC Daily Partial Column GHGs (https://www.eorc.jaxa.jp/GOSAT/GPCG/index_GOSAT.html). The GOSAT satellites can be used to monitor the global greenhouse gas distribution. They are a joint project of the Japan Aerospace Exploration Agency (JAXA), the Ministry of the Environment (MOE), and the National Institute for Environmental Studies (NIES).

The calculation method of CO$_2$ emissions in each region is given by

$$E_{CO_2} = \sum_{n=1}^{n} F_n a_n \,,$$

where E_{CO_2} is the CO$_2$ emissions, F_n is the consumption of energy n (only the primary energy is calculated here), and a_n is the corresponding emission factor (IPCC, 2019). The energy consumption data for each region in 2019 were based on the *China Energy Statistical Yearbook-2020*. We estimated the energy consumption in 2020 based on the changes in each region's industrial output value and power generation from January to February 2020 as published by China's National Bureau of Statistics (https://data.stats.gov.cn/) compared to 2019.

3.   Results and Discussion

3.1. *Changes in traffic volume reflected by changes in NO$_2$ concentrations*

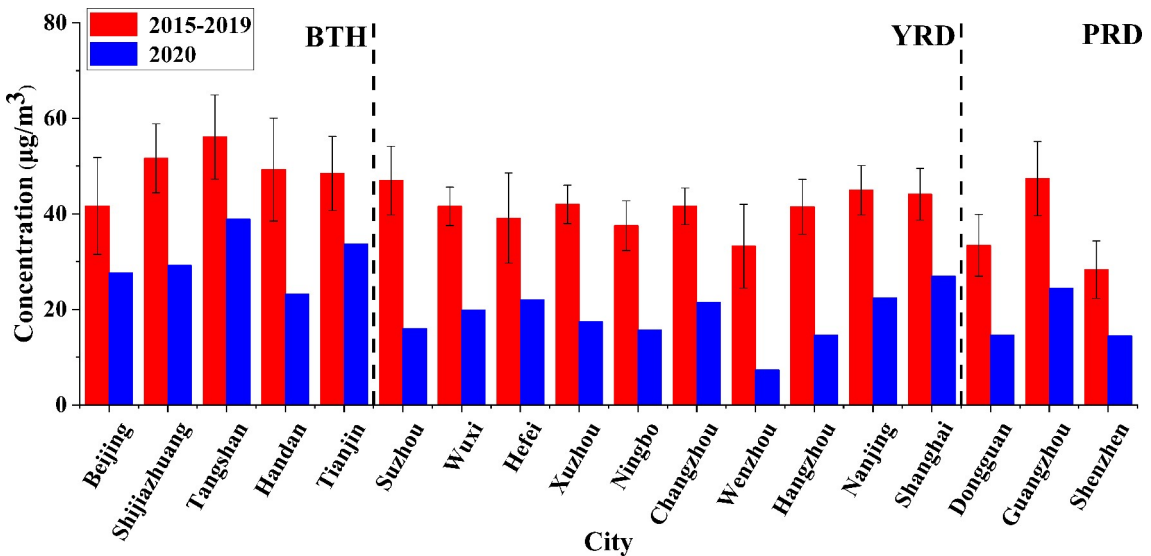Figure 2 illustrates the differences in the average concen-

Fig. 2. Average concentrations of NO$_2$ (μg m^{-3}) in major cities from 24 January to 23 February 2020 (blue bar) and the corresponding period in 2015–19 [red bar, the results are shown as the mean (±SE)] .

trations of NO_2 in 2020 and the same period in the years 2015–19 in the large cities of the three regions (BTH, the YRD, and the PRD). The NO_2 levels of all cities decreased significantly during the community lockdown in 2020 compared with previous years. Wenzhou had the highest decline at 77.89%, while the lowest decline of 30.53% was observed in Tianjin. There is a close relationship between urban NO_2 concentration and traffic volume (Anttila et al., 2011). Large traffic volumes will cause traffic congestion, and NO_2 concentrations are positively correlated with traffic congestion in the form of a power function (Shi et al., 2018). The characteristics of the NO_2 changes in large cities in 2020 are the likely result of significantly reduced traffic volumes.

The sharp decline in road passenger and cargo transportation volume also supports that the traffic dropped significantly (Table 1). For all regions, compared with the last year, the transportation volume of road passengers decreased by more than 70%. Among them, the YRD had the largest decrease of 88.63%. The transportation volume of road cargo also dropped significantly, noting that the PRD experienced the largest decrease of 64.30%.

3.2.   *Changes in PM$_{2.5}$ concentrations by city*

Changes in the $PM_{2.5}$ concentrations of large cities with similar population sizes were not consistent, but large cities in the same region showed similar changes. Figures 3–5 show the differences in average $PM_{2.5}$ concentrations between 2020 and the same period in 2015–19 in large cities for the three regions. Overall, the air quality of the PRD in all years was significantly better than that of BTH and the YRD, and the air quality of BTH was the worst of the three. The $PM_{2.5}$ concentrations in 13 major cities in the YRD and PRD urban agglomerations decreased significantly in 2020 compared with the previous years (all passed the significance test of 0.05). The decrease in $PM_{2.5}$ concentrations of the 13 large cities in the YRD and PRD varied from 27.52% to 51.34%. Among these, $PM_{2.5}$ concentrations in the 11 cities declined by more than 30% compared with previous years. The cities of Hangzhou and Wenzhou experienced the most significant declines in $PM_{2.5}$ concentrations. However, for the large cities in BTH, there was no significant decrease in $PM_{2.5}$ concentrations compared with previ-

ous years, despite significant reductions in traffic emissions. The range in $PM_{2.5}$ concentration changes was –23.82% to 22.46%. The $PM_{2.5}$ concentrations in Beijing, Tangshan, and Tianjin increased compared to the previous year by 22.46%, 5.50%, and 13.45%, respectively.

The $PM_{2.5}$ concentrations of large cities in different regions vary when residential areas are closed, and traffic is restricted. Many scholars have reached similar conclusions. During the lockdown of the communities in Shanghai, nitrate and primary aerosol concentrations decreased significantly, as did $PM_{2.5}$ concentrations (Chen et al., 2020). The increase in $PM_{2.5}$ concentrations in Beijing during this period indicates that reductions in vehicle emissions alone cannot prevent this type of pollution and that comprehensive controls are still required to improve air quality (Pei et al., 2020). During the APEC meeting held in Beijing in 2014, traffic, industry, and heating simultaneously decreased, and the concentrations of $PM_{2.5}$ in Beijing dropped significantly (Xu et al., 2019; Wang et al., 2015). Therefore, it is impossible to explain the difference in air quality changes in large cities when only traffic emissions are considered. It follows that the production of $PM_{2.5}$ in BTH is affected by other factors in addition to traffic.

A significant decrease in hourly changes in $PM_{2.5}$ concentrations compared with previous years was observed during the community lockdown in the YRD and PRD in 2020 (Fig. 6). However, this was not observed in large cities of BTH. From 1300 to 1900 LST, the average $PM_{2.5}$ concentration of large cities in BTH in 2020 was higher than in previous years. For the three major regions, there were obvious peaks (local maximums) and valleys (local minimums) in the daily time series of $PM_{2.5}$ concentrations. Peaks tended to occur after morning rush hour, between 800 and 1100 LST, and valleys were common in the afternoon, between 1300 and 1900 LST. Concentrations were generally higher at night than during the day and reached their daily minimum values in the afternoon. This result is consistent with the study of Wang et al. (2019). The hourly changes in $PM_{2.5}$ concentrations in Chinese cities show a bimodal distribution. The increased traffic volume combined with the shallow inversion layer contributes to the first-morning peak. A second peak occurs late at night into early morning. One of the reasons for this is that low electricity prices at night lead

Table 1.   Changes in road-passenger traffic and cargo traffic in February 2020 compared with the same period of 2019.

	Area	Transportation volume of road passengers (10^4)	Change from last year	Transportation volume of road cargo (10^7 kg)	Change from last year
BTH	Beijing	818	–76.25%	726	–29.72%
	Tianjin	192	–79.11%	1253	–45.31%
	Hebei	65	–97.61%	5130	–37.74%
YRD	Shanghai	2	–99.32%	2200	–21.09%
	Jiangsu	1181	–84.72%	3869	–47.77%
	Zhejiang	397	–94.06%	3511	–38.04%
	Anhui	602	–86.57%	6981	–36.52%
PRD	Guangdong	2010	–78.60%	7098	–64.30%
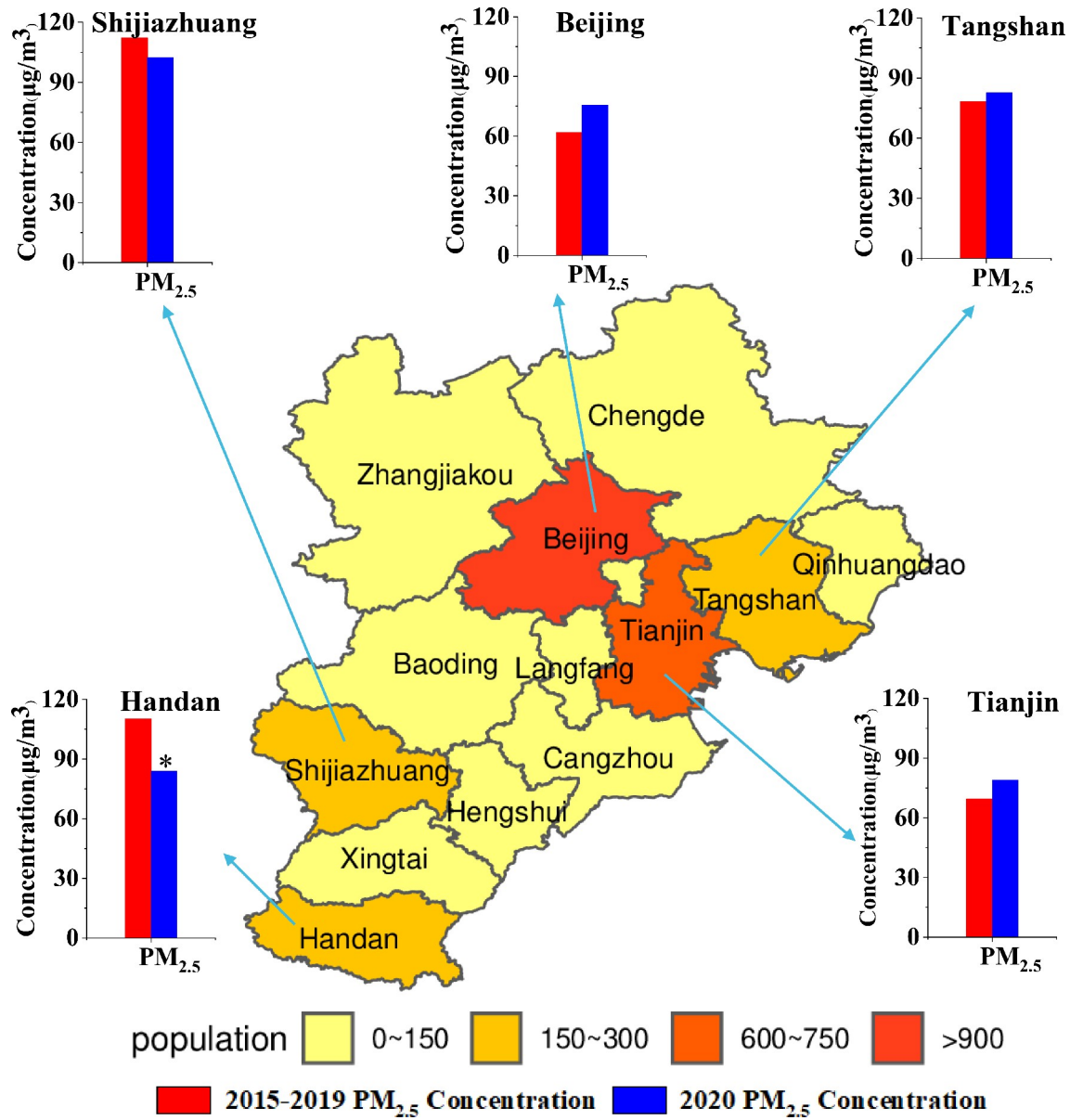
Fig. 3. Populations of the BTH urban areas (filled) and $PM_{2.5}$ concentrations (blue bars) during the lockdown of residential areas in large cities in 2020, compared with the same period in previous years (2015–19) (red bars) (* denotes having passed a 0.05 significance test).

to more emissions from industrial activities. The strongest reduction occurs in the afternoon when declining traffic volume and enhanced atmospheric convective motion favor lower $PM_{2.5}$ concentrations (Wang et al., 2019).

In 2020, the peak and valley values in the YRD and PRD were all significantly lower than those in previous years. The peak values decreased by 28.26 μg m^{-3} and 19.04 μg m^{-3}, respectively, and the valley values decreased by 23.57 μg m^{-3} and 14.25 μg m^{-3}. Resmi et al. (2020) studied the daily changes in $PM_{2.5}$ levels in Kannur and Kerala, India, during the lockdown of those cities. They observed similar afternoon declines, which were also attributed to reduced vehicle emissions.

There are some differences between the hourly changes

of $PM_{2.5}$ concentrations in 2020 and those observed in previous years. Compared with previous years, the peak and valley values of $PM_{2.5}$ in the three regions in 2020 were closer; consequently, the ranges of values is lower. In particular, the drop in the peak is less than the drop in the valley. Again, this observation is consistent with a sharp drop in traffic volume (Table 1) and a consequent reduction in vehicle emissions during the morning and evening rush hours. Furthermore, in BTH, from 1300 to 1900 LST, the valley values of $PM_{2.5}$ concentrations in 2020 were higher than in previous years. This may be related to a shallower boundary layer and stable atmospheric stratification (Wang et al., 2020) in BTH. In 2020, the nighttime $PM_{2.5}$ concentration of BTH decreased only slightly, likely related to human activ-
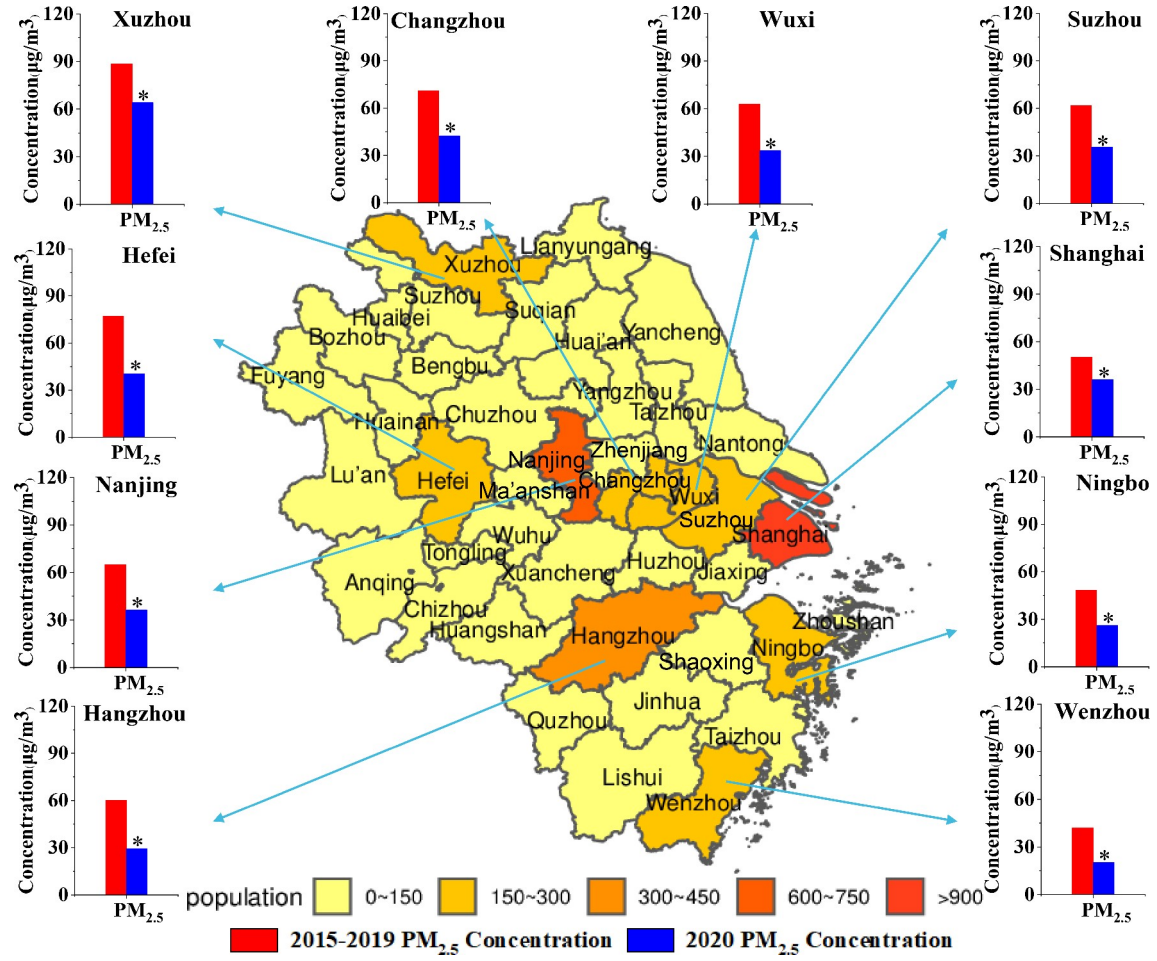
Fig. 4. Same as Fig. 3, but for the YRD.

ities that did not stop completely (Cui et al., 2020).

3.3. *Impact of industrial activities on the PM$_{2.5}$ concentration change*

During the lockdown of communities in 2020, the degree of industrial activities (Fig. 7a) changed. These changes were compared with the same one-month period in 2019 (Fig. 7b). The cumulative FRP value during this period in 2020 reveals that more industrial thermal anomalies and overall higher values were observed in northern China compared to southern China. In contrast to southern China, industrial operations in northern China remained active during the city lockdown, and they were even more active than in previous years. Compared with 2019, the number of fire spots in BTH increased by 66.10% in 2020, and the total FRP value increased by 52.73%. This is likely attributed to a greater demand for heating requirements and a higher concentration of heavy industry in northern China. During this period, industrial activities in BTH were mainly concentrated in Tangshan, with Handan being most active in southern Hebei Province. Industries in Shanxi and Shandong around the BTH region remained very active, and areas of large FRP values were found in both provinces. Central Shanxi and Tangshan in Hebei Province are major coal

mining regions, where the more intensive industrial activities are associated with energy production. In contrast, the intensity of industrial activities in the YRD was relatively weak and limited to the industrial cities in Xuzhou city, southern Anhui Province, and southern Jiangsu Province. The PRD had the lowest level of industrial activity among the three major regions.

The intensity of industrial activities in most parts of China decreased significantly in 2020 compared with the same period in 2019 (Fig. 7b); however, the industrial activities in Shanxi, most parts of Shandong, southern Hebei, and some parts of Tianjin were more intense in 2020 than in 2019. Overall, the change in industrial activities for the three regions in 2020 was essentially the same as the change in PM$_{2.5}$ concentrations in each large city. Considering that traffic emissions generally decreased, this finding suggests that the altered industrial emissions were the primary reason for the differences in the PM$_{2.5}$ concentration changes for the different regions. Zhang et al. (2019) analyzed satellite-observed data of China's industrial heat sources and found that the industrial heat radiation flux density was highly correlated to PM$_{2.5}$ concentrations, indicating that the intensity of industrial activities affected the air quality of many cities in China. Research based on the meteorology-chemistry
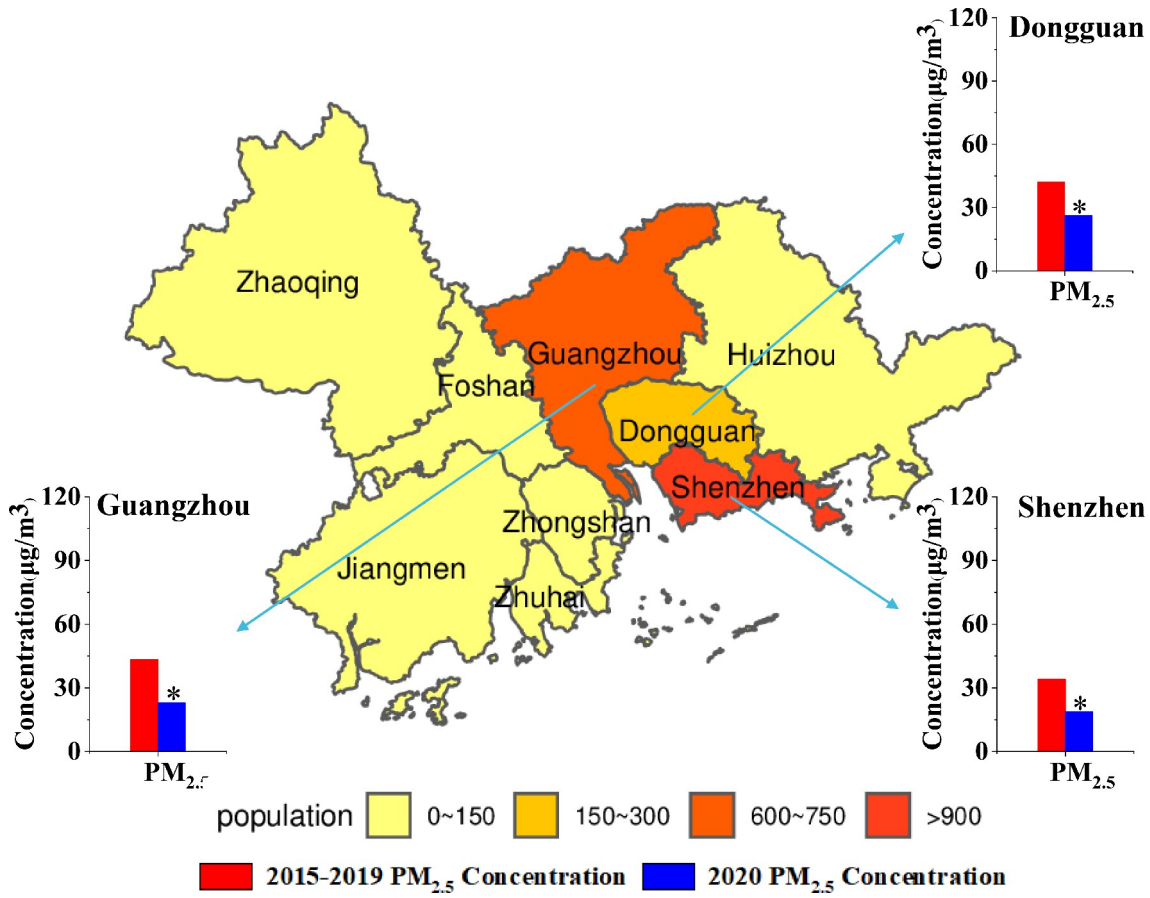
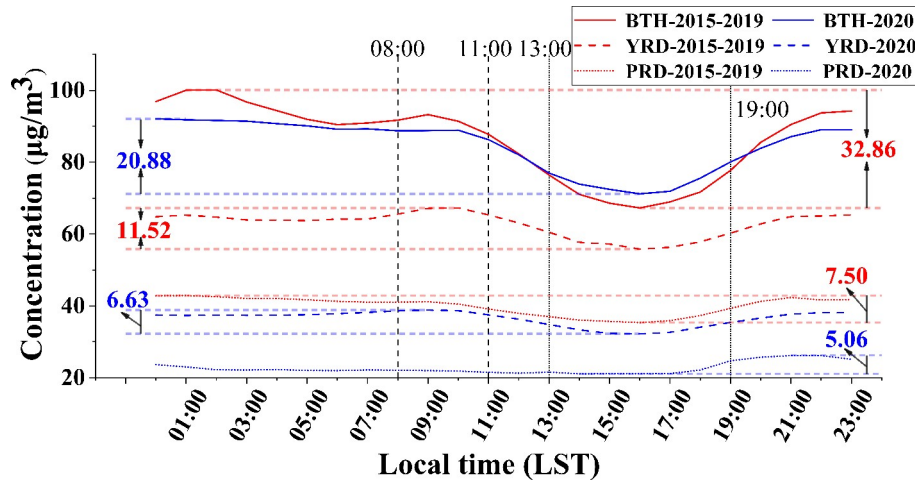**Fig. 5.** Same as Fig. 3 but for the PRD.

Fig. 6. Comparison of hourly-averaged PM$_{2.5}$ concentrations during the lockdown of residential areas in major cities in 2020 and for the same period in previous years (2015–19). The BTH, YRD, and PRD regions are represented by solid lines, dashed lines, and short dotted lines, respectively. Horizontal dashed lines mark the peak and valley for each area. The differences between the peaks and valleys (range of values) are also marked on the left side of the figure. Blue and red distinguish 2020 from the previous years (2015–19), respectively.

model (Gao et al., 2018) also confirmed that China's power and industry sectors are the main sources of aerosol emissions. Changes in the intensity of industrial activities in the BTH, YRD, and PRD are closely related to PM$_{2.5}$ concentrations.

In addition to the possible contribution of local heating and industrial emissions (Nichol et al., 2020), the PM$_{2.5}$ concentration in BTH is also affected by the transmission of pol-
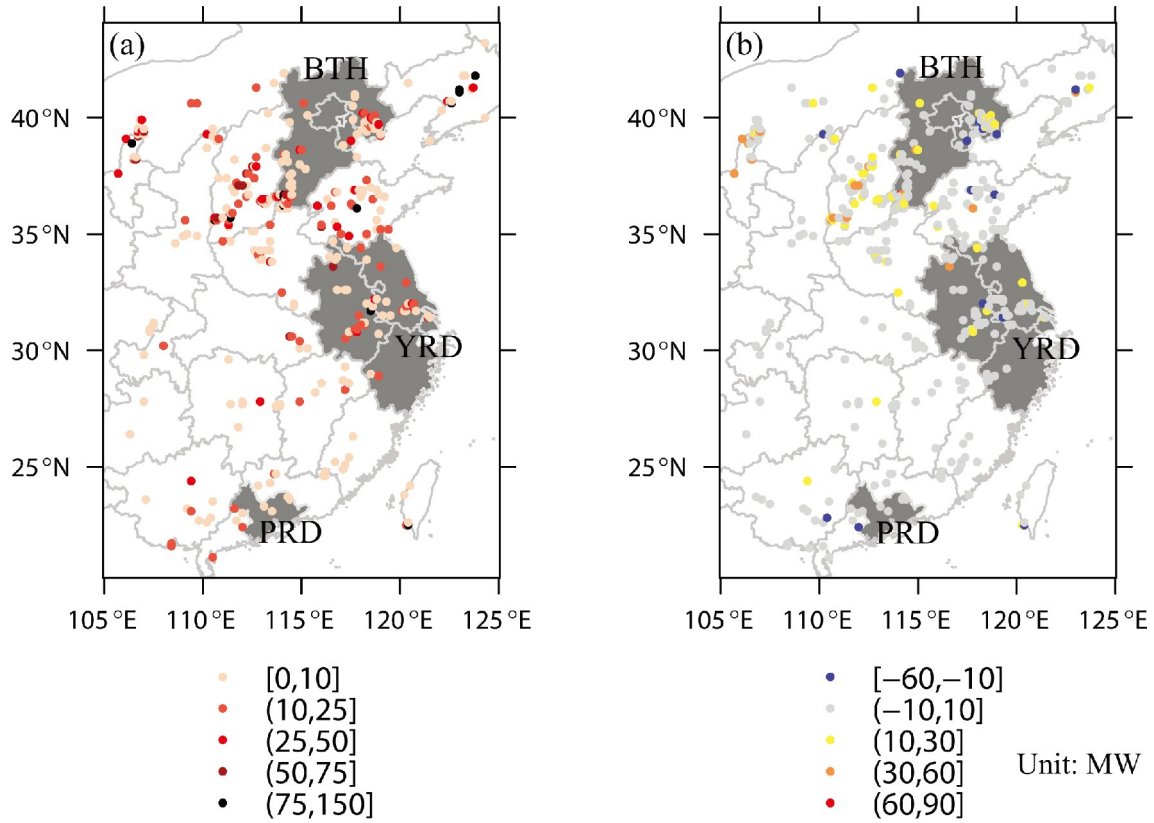
Fig. 7. Industrial activity in major urban agglomerations in China during the lockdown of residential areas in 2020. (a) The cumulative FRP values of China's major urban agglomerations (units: MW) from 24 January 2020 to 23 February 2020; (b) The difference, for the years 2020 and 2019, between the cumulative FRP values of China's major urban agglomerations for the same period 24 January to 23 February (2020–19) (units: MW). The areas filled with gray are the BTH, YRD, and PRD. The point represents the sum of the FRP value of the fire point in the area of $0.1° \times 0.1°$.

lutants across regions. Zhao et al. (2020) analyzed the sources of two pollution incidents in BTH during a city block-ade: local emissions and short-distance transmission of sur-rounding air masses (Zhao et al., 2020). The FRP value sup-ports this analysis (Fig. 7). In 2020, there were more intense industrial activities in central Shandong, central Henan, north-ern Shaanxi, and Shanxi provinces than in 2019, which provides opportunities for the transmission of pollutants into BTH. This supports the premise that in the context of par-tial emission reduction, coordinated emission reduction among various regions is important for preventing and con-trolling pollution.

Figure 8a illustrates the profit per unit area of mining and manufacturing in the three regions. The mining profit per unit area in BTH was more than three times higher than that of the YRD and the PRD. The manufacturing profit per unit area in BTH was considerably lower than that of the other two regions, about half of that of either the YRD or PRD. These differences may be related to the different geo-graphical locations and historical development of the three major regions. While residential areas were in lockdown, some manufacturing industries shut down. However, owing to heating and power requirements, the energy supply could not be interrupted, so the mining industry remained opera-

tional. Consequently, although the industrial activities were weakened, they were still ongoing in BTH and other surround-ing cities in northern China, resulting in the persistent indus-trial emissions of $PM_{2.5}$. The thermal power anomaly illus-trated in Fig. 7 provides further evidence for this conclu-sion.

Further energy production per unit area and composi-tion are shown in Fig. 8b. The output of total energy, coke, and raw coal per unit area in the BTH was significantly higher than that of the YRD and the PRD. Chinese coal mines are mainly concentrated in the north. The raw coal pro-duction in the BTH and the YRD accounts for most of the energy sources extracted in these regions, while few raw coal mining activities took place in the PRD. The lower energy extraction level in the PRD was conducive to reduced $PM_{2.5}$ emissions. Regardless, emissions from coal-fired heating have exacerbated pollution, most especially in northern China (Xiao et al., 2015; Si et al., 2019).

Thermal power is also an important source of urban pollu-tion (Tan et al., 2020). The three regions are all dominated by thermal power generation, accounting for 73.94%–98.76% of the total power generation (Fig. 8c). Clean energy (nu-clear power, wind power, and solar power) generation accounts for the smallest proportion of total power genera-
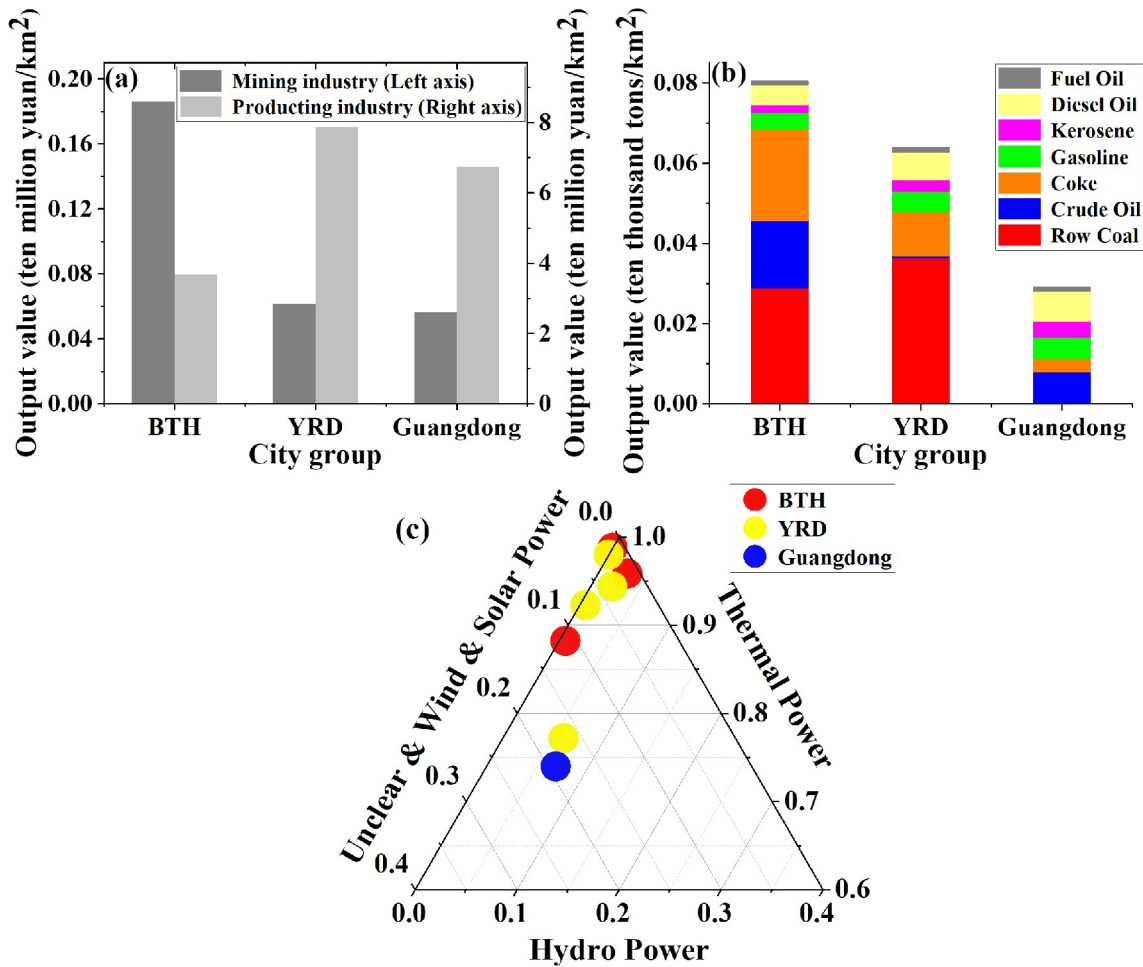
Fig. 8. Industrial structure and energy output and supply of the three major urban agglomerations (representing the PRD in Guangdong Province), (a) Mining (dark gray) and manufacturing (light gray) profits (industrial sales output value of the year) per unit area cluster of the three major urban agglomerations; (b) energy output per unit area of the three major urban agglomerations; (c) a ternary phase diagram of the proportion of the power generation composition of the provinces in the three major urban agglomerations.

tion. The thermal power generation of the three regions accounts for more than 85.79% of the total power generation. Guangdong Province has the lowest proportion of thermal power generation and the highest proportion of clean energy generation of all provinces in the three regions. The electric power sector is among the sectors that emit the most pollutants (Jorgenson et al., 2016; Tong et al., 2018), and the burning of fossil fuels for thermal power generation is one of the main causes of pollution. The increased use of clean power generation favors a reduction in $PM_{2.5}$ emissions. Conversely, a larger proportion of thermal power generation in BTH regions is conducive to increased $PM_{2.5}$ emissions.

3.4. *Meteorological conditions*

Meteorological conditions are also an important factor affecting $PM_{2.5}$ concentrations in urban agglomerations. The bubble chart in Fig. 9 shows the distribution of the ground temperature, humidity, and wind speed of large cities in the three regions during the city lockdown in 2020

and for the same one-month period in previous years (2015–19). As Fig. 9a illustrates, the distribution of meteorological elements in the BTH urban agglomeration was relatively concentrated in previous years. The temperatures and relative humidity were mostly near 0°C and below 50%, respectively, while wind speeds were between 1–3 m s^{-1}. In contrast, the temperature and humidity distribution in BTH was more dispersed during the 31-day community lockdown in 2020, and the near-surface wind speeds were significantly lower than in previous years. The average wind speed over the 31 days in 2020 was 1.90 m s^{-1}, while the average wind speed in previous years was 2.24 m s^{-1}. In comparison, the distributions of meteorological conditions in large cities in the YRD and the PRD in 2020 were remarkably similar to those in previous years. Backward trajectories also show that the transmission and diffusion of air masses reaching the BTH was weaker than that of the YRD and the PRD [Fig. S1 in the electronic supplementary material (ESM)].

In general, unfavorable meteorological conditions aggravated the impact of industrial emissions in the BTH region
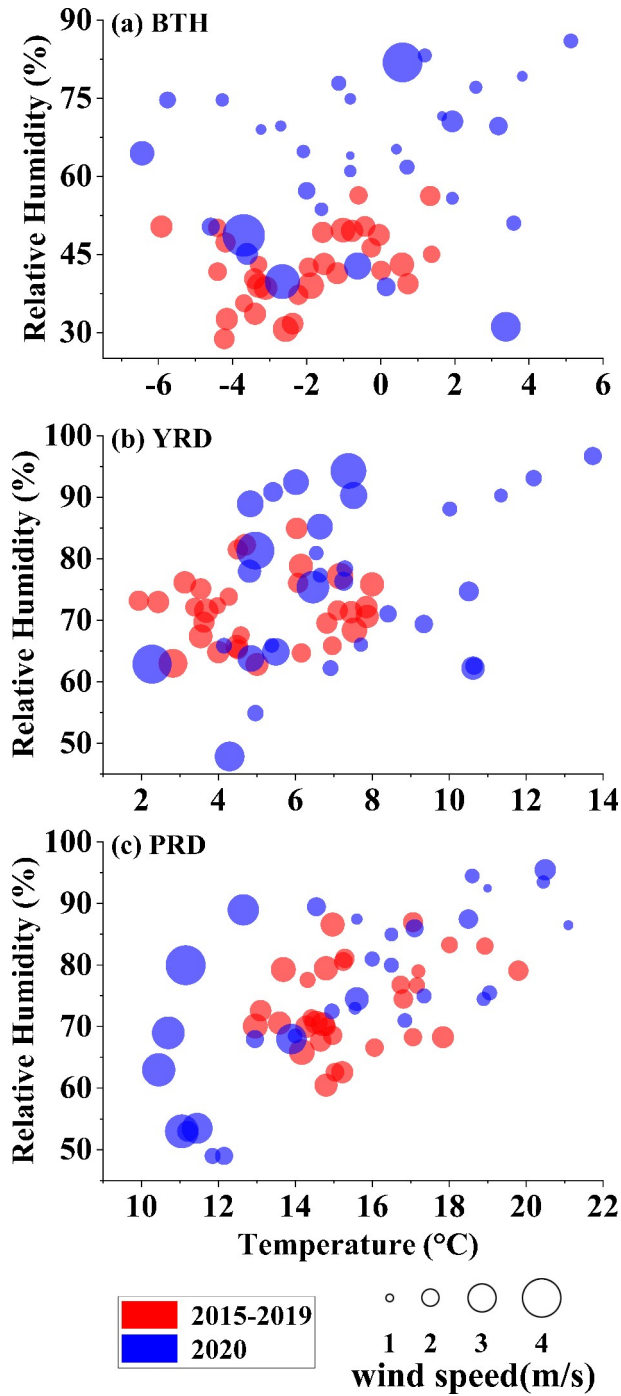
Fig. 9. Bubble charts of meteorological elements (temperature, relative humidity, and surface wind speed) of the large cities of the three major urban agglomerations during the 2020 city lockdown (blue bubbles) and the same period in previous years (2015–19) (red bubbles) (a) BTH; (b) YRD; (c) PRD.

and its surrounding cities, resulting in higher $PM_{2.5}$ concentrations in the large cities. The research of Wang et al. (2020) and Sulaymon et al. (2021) also proves this. Lower wind speeds in BTH make it more difficult for air pollutants to spread. Higher relative humidity and warmer temperatures accelerate chemical reactivity, thereby accelerating the formation of secondary particles. At the same time, the lower planet-

ary boundary layer height also inhibits pollutant diffusion. The lack of precipitation makes it impossible for $PM_{2.5}$ to be eliminated by wet deposition (Sulaymon et al., 2021). For the YRD and the PRD, there were no obvious unfavorable weather conditions. The meteorological conditions of the YRD and PRD had a limited impact on the changes in pollutant concentrations (Liu et al., 2021; Wen et al., 2022). Average weather conditions coupled with a reduction of industrial activities and traffic volume in 2020 caused a significant reduction in $PM_{2.5}$ concentration compared with previous years. It follows that meteorological conditions can potentially exacerbate $PM_{2.5}$ concentrations, as they did in BTH in 2020. However, the meteorology may not be the primary reason for the relatively high $PM_{2.5}$ concentration. Even under unfavorable weather conditions, strict control of pollutant emissions can still be expected to reduce $PM_{2.5}$ pollution levels (Mahato et al., 2020).

3.5. *Changes in CO_2 emissions and environmental CO_2 concentrations*

During the city lockdown, CO_2 emissions fell sharply, with a decrease of nearly 20% across the country (Fig. 10a1). Among these, the CO_2 emissions from transportation have fallen the most, with a 40% reduction in 2020 compared to the same period in the last year (Figs. 10a3, a6). The reduction rate of industrial CO_2 emissions ranked second (Figs. 10a4), and the CO_2 emission reduction of residential consumption and power was the smallest (Figs. 10a5, a2). These results show that during the city lockdown, the basic livelihood of citizens was guaranteed with minimal impact. From the perspective of regional reductions in the emission of CO_2, emissions attributed to the thermal power of the YRD and the industrial activity of the PRD experienced the largest declines among the three regions, both exceeding 20% (Figs. 10b1, b2). It also proves that the intensity of industrial activity declined most significantly during the lockdown of the PRD.

However, a substantial reduction of CO_2 has not prevented an upward trend of CO_2 concentration in the environment. During the lockdown, the average CO_2 concentration in China was 411.85 ppmv, which was still higher than the 409.89 ppmv in the same period last year, and the CO_2 concentration of the three regions also rose slightly (Fig. 10c). Unlike particulate matter, which has a short lifetime and often has a timescale of "days" (Wang et al., 2013), CO_2 has a perturbation lifetime of hundreds of years or even thousands of years (Montenegro et al., 2007). A sizeable part of the anthropogenic CO_2 emissions remains in the atmosphere, waiting for the weathering process or the deposition of $CaCO_3$ to return it to the solid earth, and these processes are quite slow (Archer et al., 2009). Therefore, the consequences of CO_2 emissions will continue for many years, and their concentration is difficult to reduce through short-term emission reductions. China's GDP and CO_2 emissions have a strong correlation, which indicates that economic growth still relies heavily on the burning of fossil fuels (Fig. 10d). With the city lockdown lifted and the restora-
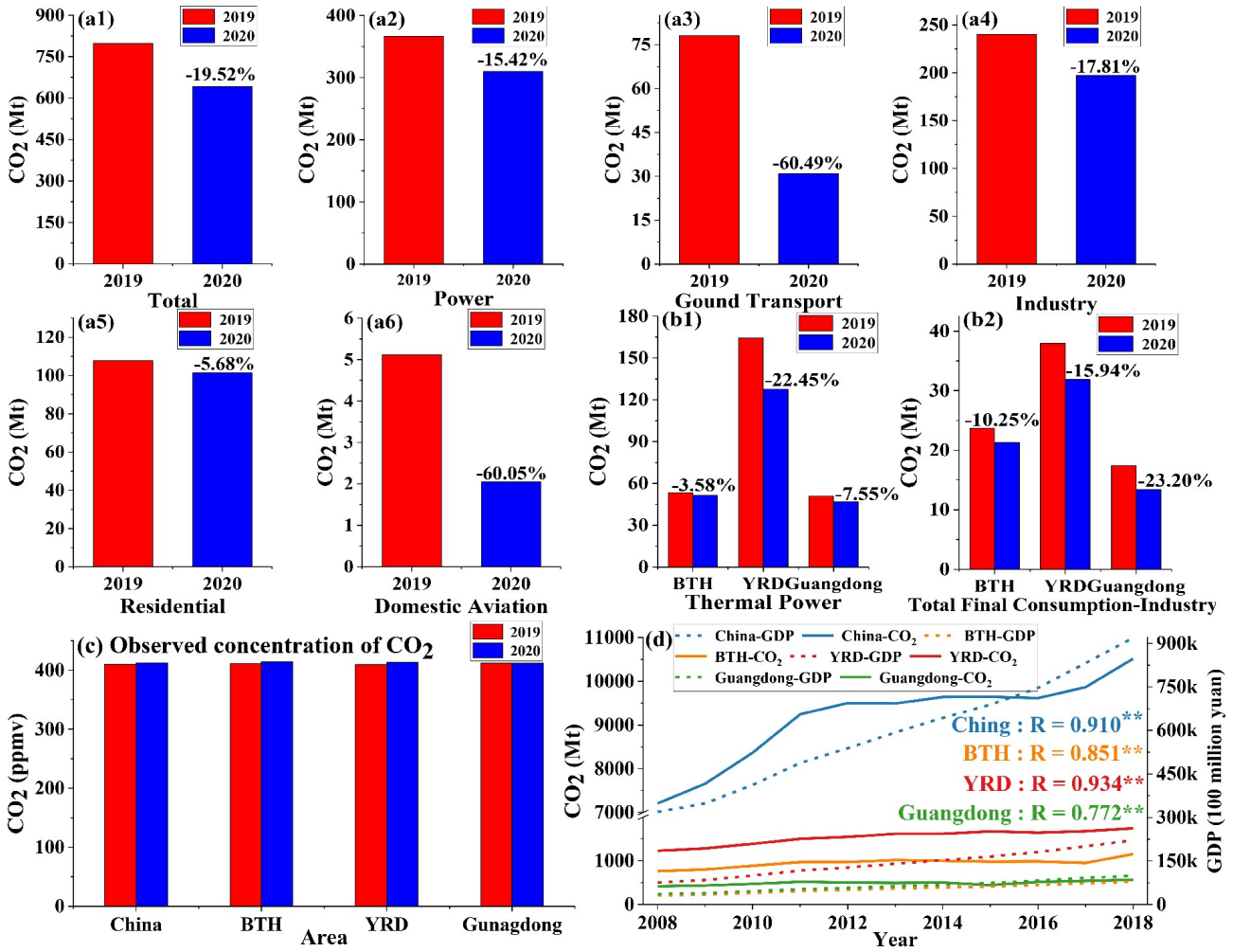
Fig. 10. CO_2 emissions and changes in environmental concentration (a1–a6, CO_2 emissions in general and by sector in China from 24 January to 23 February 2019 and 2020; b1–b2, CO_2 emissions from thermal power and industrial activities in BTH, YRD, and PRD (representing the PRD in Guangdong Province) in January and February 2019 and 2020; (c) the average CO_2 concentration observed from 24 January to 23 February 2019 and 2020; (d) CO_2 emissions and GDP changes from 2008 to 2018. The correlation coefficient R between the two is marked; ** indicates that the correlation has passed the 0.01 test.

tion of production, CO_2 emissions will rebound (Zheng et al., 2009), which shows that reducing production activities is not an effective long-term strategy for reducing CO_2 emissions. However, significantly improving energy efficiency, using clean energy, and developing high-tech industries as the main direction of economic growth do represent effective measures to reduce CO_2 emissions.

4. Conclusion

Evidence from the lockdown of cities in China shows that human activities in the transportation and industrial sectors significantly impact $PM_{2.5}$ pollution and CO_2 emissions. The results show that the concentrations of $PM_{2.5}$ in the large cities in the YRD and the PRD underwent a significant reduction during this period, decreasing by 41.87% (51.34%–27.52%) and 43.30% (47.15%–37.87%) overall, respectively. However, in the BTH region, the $PM_{2.5}$ concentrations have not significantly declined compared with previ-

ous years, decreasing by only 2.01% (23.82%–22.46%) overall. One possible reason for this difference is the variable industrial intensity changes among the regions. The BTH region and surrounding cities account for a larger proportion of the energy industry than the YRD and PRD. These industries could not be completely shut down during the lockdown. Another reason is different weather conditions. In 2020, the average high temperature was –0.54°C in 2020, 1.46°C higher than the average of 2015 to 2019. There was higher relative humidity, 63.08% in 2020, 20.42% higher than the average of 2015 to 2019, and a lower average wind speed, 1.90 m s^{-1} in 2020, 0.34 m s^{-1} less than 2015 to 2019 average. The combined effects of the weather anomalies in BTH made it difficult for pollution to spread, thus increasing pollutant concentrations. During the city lockdown, China's CO_2 emissions dropped by 19.52% compared to the past year. The CO_2 emissions from transportation dropped the most, with ground transport and domestic aviation falling by 60.49% and 60.05%, respectively. However, the envir-

onmental CO_2 concentration did not decrease in 2020. Short-term CO_2 emission reduction cannot effectively suppress the rising trend of CO_2.

In summary, reducing air pollution requires coordinated emission reductions in transportation, industry, and other sectors, especially in the winter when pollution occurs frequently and weather conditions are not conducive to pollutant diffusion. The coordinated emission reduction of various cities favors the effective control of air pollution. Meteorological conditions affect the diffusion of pollutants and have a greater impact on the concentration of pollutants. Strengthened forecast skills favor the prevention of air pollution incidents. Improving energy efficiency, using more clean energy, and reducing the dependence of economic development on fossil fuels are effective ways to reduce CO_2 and slow down global warming.

Electronic supplementary material: Supplementary material is available in the online version of this article at https://doi.org/10.1007/s00376-021-1281-x.

REFERENCES

An, R. Y., B. Y. Yu, R. Li, and Y.-M. Wei, 2018: Potential of energy savings and CO_2 emission reduction in China's iron and steel industry. *Applied Energy*, **226**, 862−880, https://doi.org/10.1016/j.apenergy.2018.06.044.

Andreoni, V., 2021: Estimating the European CO_2 emissions change due to COVID-19 restrictions. *Science of the Total Environment*, **769**, 145115, https://doi.org/10.1016/j.scitotenv.2021.145115.

Anttila, P., J.-P., Tuovinen, and J. V. Niemi, 2011: Primary NO_2 emissions and their role in the development of NO_2 concentrations in a traffic environment. *Atmos. Environ.*, **45**, 986−992, https://doi.org/10.1016/j.atmosenv.2010.10.050.

Archer, D., and Coauthors, 2009: Atmospheric lifetime of fossil fuel carbon dioxide. *Annual Review of Earth and Planetary Sciences*, **37**, 117−134, https://doi.org/10.1146/annurev.earth.031208.100206.

Bertram, C., G. Luderer, F. Creutzig, N. Bauer, F. Ueckerdt, A. Malik, and O. Edenhofer, 2021: COVID-19-induced low power demand and market forces starkly reduce CO_2 emissions. *Nature Climate Change*, **11**, 193−196, https://doi.org/10.1038/s41558-021-00987-x.

Chen, H., J. T. Huo, Q. Y. Fu, Y. S. Duan, H. Xiao, and J. M. Chen, 2020: Impact of quarantine measures on chemical compositions of $PM_{2.5}$ during the COVID-19 epidemic in Shanghai, China. *Science of the Total Environment*, **743**, 140758, https://doi.org/10.1016/j.scitotenv.2020.140758.

Chen, L., and Z. F. Yang, 2015: A spatio-temporal decomposition analysis of energy-related CO_2 emission growth in China. *Journal of Cleaner Production*, **103**, 49−60, https://doi.org/10.1016/j.jclepro.2014.09.025.

Chu, B. W., S. P. Zhang, J. Liu, Q. X. Ma, and H. He, 2021: Significant concurrent decrease in $PM_{2.5}$ and NO_2 concentrations in China during COVID-19 epidemic. *Journal of Environmental Sciences*, **99**, 346−353, https://doi.org/10.1016/j.jes.2020.06.031.

Cui, Y., D. S. Ji, W. Maenhaut, W. K. Gao, R. J. Zhang, and Y. S. Wang, 2020: Levels and sources of hourly $PM_{2.5}$-related elements during the control period of the COVID-19 pandemic at a rural site between Beijing and Tianjin. *Science of the Total Environment*, **744**, 140840, https://doi.org/10.1016/j.scitotenv.2020.140840.

Dai, Q. L., and Coauthors, 2021: Haze episodes before and during the COVID-19 shutdown in Tianjin, China: Contribution of fireworks and residential burning. *Environmental Pollution*, **286**, 117252, https://doi.org/10.1016/j.envpol.2021.117252.

Gao, M., D. S. Ji, F. C. Liang, and Y. Liu, 2018: Attribution of aerosol direct radiative forcing in China and India to emitting sectors. *Atmos. Environ.*, **190**, 35−42, https://doi.org/10.1016/j.atmosenv.2018.07.011.

Guo, J. P., and Coauthors, 2017: Declining frequency of summertime local-scale precipitation over eastern China from 1970 to 2010 and its potential link to aerosols. *Geophys. Res. Lett.*, **44**, 5700−5708, https://doi.org/10.1002/2017GL073533.

IPCC, 2019: 2019 Refinement to the 2006 IPCC Guidelines for National Greenhouse Gas Inventories.

Jorgenson, A., W. Longhofer, and D. Grant, 2016: Disproportionality in power plants' carbon emissions: A cross-national study. *Scientific Reports*, **6**, 28661, https://doi.org/10.1038/srep28661.

Liu, H., and Coauthors, 2017: The blue skies in Beijing during APEC 2014: A quantitative assessment of emission control efficiency and meteorological influence. *Atmos. Environ.*, **167**, 235−244, https://doi.org/10.1016/j.atmosenv.2017.08.032.

Liu, L., and Coauthors, 2021: Chemistry of atmospheric fine particles during the COVID-19 pandemic in a megacity of eastern China. *Geophys. Res. Lett.*, **48**, 2020GL091611, https://doi.org/10.1029/2020GL091611.

Liu, Z., and Coauthors, 2020a: Near-real-time monitoring of global CO_2 emissions reveals the effects of the COVID-19 pandemic. *Nature Communications*, **11**, 6292, https://doi.org/10.1038/s41467-020-20254-5.

Liu, Z., and Coauthors, 2020b: Carbon Monitor, a near-real-time daily dataset of global CO_2 emission from fossil fuel and cement production. *Scientific Data*, **7**, 392, https://doi.org/10.1038/s41597-020-00708-7.

Lu, D. W., and Coauthors, 2021: COVID-19-induced lockdowns indicate the short-term control effect of air pollutant emission in 174 cities in China. *Environ. Sci. Technol.*, **55**, 4094−4102, https://doi.org/10.1021/acs.est.0c07170.

Ma, C. H., J. Yang, F. Chen, Y. Ma, J. B. Liu, X. P. Li, J. B. Duan, and R. Guo, 2018: Assessing heavy industrial heat source distribution in China using real-time VIIRS active fire/hotspot data. *Sustainability*, **10**, 4419, https://doi.org/10.3390/su10124419.

Mahato, S., S. Pal, K.G. Ghosh, 2020: Effect of lockdown amid COVID-19 pandemic on air quality of the megacity Delhi, India. *Science of The Total Environment*, **730**, 139086, https://doi.org/10.1016/j.scitotenv.2020.139086.

Montenegro, A., V. Brovkin, M. Eby, D. Archer, and A. J. Weaver, 2007: Long term fate of anthropogenic carbon. *Geophys. Res. Lett.*, **34**, L19707, https://doi.org/10.1029/2007GL030905.

Nichol, J. E., M. Bilal, M. A. Ali, and Z. F. Qiu, 2020: Air pollution scenario over China during COVID-19. *Remote Sensing*, **12**, 2100, https://doi.org/10.3390/rs12132100.

Pei, Z. P., G. Han, X. Ma, H. Su, and W. Gong, 2020: Response of major air pollutants to COVID-19 lockdowns in China. *Science of the Total Environment*, **743**, 140879, https://doi.org/10.1016/j.scitotenv.2020.140879.

Resmi, C. T., T. Nishanth, M. K. Satheesh Kumar, M. G. Manoj, M. Balachandramohan, and K. T. Valsaraj, 2020: Air quality improvement during triple-lockdown in the coastal city of Kannur, Kerala to combat Covid-19 transmission. *PeerJ*, **8**, e9642, https://doi.org/10.7717/peerj.9642.

Schroeder, W., P. Oliva, L. Giglio, and I. A. Csiszar, 2014: The New VIIRS 375m active fire detection data product: Algorithm description and initial assessment. *Remote Sensing of Environment*, **143**, 85−96, https://doi.org/10.1016/j.rse.2013.12.008.

Shan, Y. L., and Coauthors, 2018: China CO_2 emission accounts 1997–2015. *Scientific Data*, **5**, 170201, https://doi.org/10.1038/sdata.2017.201.

Shan, Y. L., Q. Huang, D. B. Guan, and K. Hubacek, 2020: China CO_2 emission accounts 2016–2017. *Scientific Data*, **7**, 54, https://doi.org/10.1038/s41597-020-0393-y.

Shan, Y. L., J. H. Liu, Z. Liu, X. W. H. Xu, S. Shao, P. Wang, and D. B. Guan, 2016: New provincial CO_2 emission inventories in China based on apparent energy consumption data and updated emission factors. *Applied Energy*, **184**, 742−750, https://doi.org/10.1016/j.apenergy.2016.03.073.

Shi, K., B. F. Di, K. S. Zhang, C. Y. Feng, and L. Svirchev, 2018: Detrended cross-correlation analysis of urban traffic congestion and NO_2 concentrations in Chengdu. *Transportation Research Part D: Transport and Environment*, **61**, 165−173, https://doi.org/10.1016/j.trd.2016.12.012.

Si, Y. D., H. M. Wang, K. Cai, L. F. Chen, Z. C. Zhou, and S. S. Li, 2019: Long-term (2006–2015) variations and relations of multiple atmospheric pollutants based on multi-remote sensing data over the North China Plain. *Environmental Pollution*, **255**, 113323, https://doi.org/10.1016/j.envpol.2019.113323.

Sovacool, B. K., D. F. Del Rio, and S. Griffiths, 2020: Contextualizing the Covid-19 pandemic for a carbon-constrained world: Insights for sustainability transitions, energy justice, and research methodology. *Energy Research & Social Science*, **68**, 101701, https://doi.org/10.1016/j.erss.2020.101701.

Sulaymon, I. D., and Coauthors, 2021: Persistent high $PM_{2.5}$ pollution driven by unfavorable meteorological conditions during the COVID-19 lockdown period in the Beijing-Tianjin-Hebei region, China. *Environ. Res.*, **198**, 111186, https://doi.org/10.1016/j.envres.2021.111186.

Sun, J. Q., Y. X. Liu, Y. Z. Dong, B. H. Xu, and X. L. Wei, 2018: Classification of urban industrial heat sources based on Suomi-NPP VIIRS nighttime thermal anomaly products: A case study of the Beijing-Tianjin-Hebei region. *Geography and Geo-Information Science*, **34**, 13−19, https://doi.org/10.3969/j.issn.1672-0504.2018.03.003. (in Chinese with English abstract)

Sun, S., L. J. Li, Z. H. Wu, A. Gautam, J. X. Li, and W. J. Zhao, 2020: Variation of industrial air pollution emissions based on VIIRS thermal anomaly data. *Atmospheric Research*, **244**, 105021, https://doi.org/10.1016/j.atmosres.2020.105021.

Tan, W., C. Liu, S. S. Wang, H. R. Liu, Y. Z. Zhu, W. J. Su, Q. H. Hu, and J. G. Liu, 2020: Long-distance mobile MAX-DOAS observations of NO_2 and SO_2 over the North China Plain and identification of regional transport and power plant emissions. *Atmospheric Research*, **245**, 105037, https://doi.org/10.1016/j.atmosres.2020.105037.

Tang, M. L., D. Li, Z. Liew, F. Wei, J. B. Wang, M. J. Jin, K. Chen, and B. Ritz, 2020: The association of short-term effects of air pollution and sleep disorders among elderly residents in China. *Science of the Total Environment*, **708**, 134846, https://doi.org/10.1016/j.scitotenv.2019.134846.

Tong, D., and Coauthors, 2018: Targeted emission reductions from global super-polluting power plant units. *Nature Sustainability*, **1**, 59−68, https://doi.org/10.1038/s41893-017-0003-y.

Tsidulko, M., I. A. Csiszar, W. Schroeder, R. Ahmadov, E. James, and G. Pereira, 2018: Improving VIIRS fire radiative power estimates for smoke emission modeling applications. *AGU Fall Meeting Abstracts*, AGU.

Wang, J. Z., Y. Q. Wang, H. Liu, Y. Q. Yang, X. Y. Zhang, Y. Li, Y. M. Zhang, and G. Deng, 2013: Diagnostic identification of the impact of meteorological conditions on $PM_{2.5}$ concentrations in Beijing. *Atmos. Environ.*, **81**, 158−165, https://doi.org/10.1016/j.atmosenv.2013.08.033.

Wang, P. F., K. Y. Chen, S. Q. Zhu, P. Wang, and H. L. Zhang, 2020: Severe air pollution events not avoided by reduced anthropogenic activities during COVID-19 outbreak. *Resources, Conservation and Recycling*, **158**, 104814, https://doi.org/10.1016/j.resconrec.2020.104814.

Wang, S. X., and Coauthors, 2010: Quantifying the air pollutants emission reduction during the 2008 Olympic Games in Beijing. *Environ. Sci. Technol.*, **44**, 2490−2496, https://doi.org/10.1021/es9028167.

Wang, S. H., Y. G. Zhang, J. Hakkarainen, W. M. Ju, Y. X. Liu, F. Jiang, and W. He, 2018: Distinguishing anthropogenic CO_2 emissions from different energy intensive industrial sources using OCO-2 observations: A case study in northern China. *J. Geophys. Res.: Atmos.*, **123**, 9462−9473, https://doi.org/10.1029/2018JD029005.

Wang, Y. Z., X. J. Duan, and L. Wang, 2019: Spatial-temporal evolution of $PM_{2.5}$ concentration and its socioeconomic influence factors in Chinese cities in 2014–2017. *International Journal of Environmental Research and Public Health*, **16**, 985, https://doi.org/10.3390/ijerph16060985.

Wang, Z. S., and Coauthors, 2015: Changes in atmospheric composition during the 2014 APEC conference in Beijing. *J. Geophys. Res.: Atmos.*, **120**, 12695−12707, https://doi.org/10.1002/2015JD023652.

Wen, L. Y., and Coauthors, 2022: Investigation of $PM_{2.5}$ pollution during COVID-19 pandemic in Guangzhou, China. *Journal of Environmental Sciences*, **115**, 443−452, https://doi.org/10.1016/j.jes.2021.07.009.

Xiao, Q. Y., Z. W. Ma, S. S. Li, and Y. Liu, 2015: The impact of winter heating on air pollution in China. *PLoS ONE*, **10**,

e0117311, https://doi.org/10.1371/journal.pone.0117311.

Xu, W., and Coauthors, 2019: Impact of emission controls on air quality in Beijing during APEC 2014: Implications from water-soluble ions and carbonaceous aerosol in $PM_{2.5}$ and their precursors. *Atmos. Environ.*, **210**, 241−252, https://doi.org/10.1016/j.atmosenv.2019.04.050.

Yao, L. Q., and Coauthors, 2021: Co-benefits of reducing $PM_{2.5}$ and improving visibility by COVID-19 lockdown in Wuhan. *npj Climate and Atmospheric Science*, **4**, 40, https://doi.org/10.1038/s41612-021-00195-6.

Yuan, R. Q., X. Tao, and X. L. Yang, 2019: CO_2 emission of urban passenger transportation in China from 2000 to 2014. *Advances in Climate Change Research*, **10**, 59−67, https://doi.org/10.1016/j.accre.2019.03.005.

Zhang, P., and Coauthors, 2019: Satellite-based detection and char-acterization of industrial heat sources in China. *Environ. Sci. Technol.*, **53**, 11031−11042, https://doi.org/10.1021/acs.est.9b02643.

Zhao, N., G. Wang, G. H. Li, J. L. Lang, and H. Y. Zhang, 2020: Air pollution episodes during the COVID-19 outbreak in the Beijing–Tianjin–Hebei region of China: An insight into the transport pathways and source distribution. *Environmental Pollution*, **267**, 115617, https://doi.org/10.1016/j.envpol.2020.115617.

Zheng, J. Y., M. Shao, W. W. Che, L. J. Zhang, L. J. Zhong, Y. H. Zhang, and D. Streets, 2009: Speciated VOC emission inventory and spatial patterns of ozone formation potential in the Pearl River Delta, China. *Environ. Sci. Technol.*, **43**, 8580−8586, https://doi.org/10.1021/es901688e.